Nuclear Instruments and Methods in Physics Research A 631 (2011) 80–89

Contents lists available at ScienceDirect

Nuclear Instruments and Methods in Physics Research A

journal homepage: www.elsevier.com/locate/nima

Polarized neutron beam properties for measuring parity-violating spin rotation in liquid ^{4}He

A.M. Micherdzinska [a,b,*], C.D. Bass [a,d], T.D. Bass [a], K. Gan [b], D. Luo [a], D.M. Markoff [c], H.P. Mumm [d], J.S. Nico [d], A.K. Opper [b], E.I. Sharapov [e], W.M. Snow [a], H.E. Swanson [f], V. Zhumabekova [g]

[a] Indiana University/IU Center for Exploration of Energy and Matter, Bloomington, IN 47408, USA
[b] The George Washington University, Washington, DC 20052, USA
[c] North Carolina Central University, Durham, NC 27707, USA
[d] National Institute of Standards and Technology, Gaithersburg, MD 20899, USA
[e] Joint Institute for Nuclear Research, Dubna 141980, Russia
[f] University of Washington/CENPA, Seattle, WA 98195, USA
[g] Al-Farabi Kazakh National University, Al-Farabi Ave. 71, 050038 Almaty, Kazakhstan

ARTICLE INFO

Article history:
Received 5 May 2010
Received in revised form
23 November 2010
Accepted 24 November 2010
Available online 14 December 2010

Keywords:
Cold neutrons
Polarized neutrons
Neutron polarimetry
Liquid helium
Nucleon–nucleon weak interaction
Parity violation

ABSTRACT

Measurements of parity-violating neutron spin rotation can provide insight into the poorly understood nucleon–nucleon weak interaction. Because the expected rotation angle per unit length is small (10^{-7} rad/m), several properties of the polarized cold neutron beam phase space and the neutron optical elements of the polarimeter must be measured to quantify possible systematic effects. This paper presents (1) an analysis of a class of possible systematic uncertainties in neutron spin rotation measurements associated with the neutron polarimetry, and (2) measurements of the relevant neutron beam properties (intensity distribution, energy spectrum, and the product of the neutron beam polarization and the analyzing power as a function of the beam phase space properties) on the NG-6 cold neutron beam-line at the National Institute of Standards and Technology Center for Neutron Research. We conclude that the phase space nonuniformities of the polarimeter in this beam are small enough that a parity-violating neutron spin rotation measurement in n-^{4}He with systematic uncertainties at the 10^{-7} rad/m level is possible.

1. Parity-violating neutron spin rotation and theoretical motivation

Parity violation in the weak interaction between neutrons and nuclei can cause the spin of a transversely polarized neutron moving through matter to corkscrew. From a neutron optical viewpoint, this phenomenon is caused by the presence of a helicity-dependent neutron index of refraction. The index of refraction n of a medium can be expressed in terms of the coherent forward scattering amplitude $f(0)$

$$n = 1-\frac{2\pi\rho f(0)}{k^2} \tag{1}$$

where $\vec{k}$ is the incident neutron wave vector and ρ is the number density of scatterers in the medium. At low energy (in the limit $kr \ll 1$ with r the range of the neutron interaction with nucleus), $f(0)$ is the sum of two terms in an unpolarized medium: a parity-conserving (PC) term f_{PC} dominated by the strong interaction and consisting of s-waves, and a parity-violating (PV) term f_{PV} that contains only weak interactions and is dominated by a p-wave contribution. f_{PV} is proportional to $\vec{\sigma}_n \cdot \vec{k}_n$ ($\vec{\sigma}_n$ is the neutron spin vector) and so has opposite signs for positive and negative helicity neutron spin states. As a neutron moves a distance z in the medium, the forward transmission amplitudes of the two helicity states accumulate different phases: $\phi_{\pm} = \phi_{PC} \pm \phi_{PV}$. ϕ_{PV} causes a relative phase shift of the two neutron helicity components and therefore a rotation of the neutron polarization about its momentum. Because the parity-violating amplitude is proportional to k, the rotary power (spin rotation angle per unit length) $d\varphi/dz = 4\pi\rho f_{PV}/k$ tends to a constant for low energy neutrons [1].

Measurements of the weak interaction between nucleons can be used to address important questions in strong interaction physics. Measurements of parity-violating neutron spin rotation in light nuclei such as H, D, and ^{4}He [2,3] offer the opportunity to constrain nucleon–nucleon (NN) weak couplings. The expected range of the parity-violating rotation angles for such few-body systems lies in the range 10^{-6}–10^{-7} rad/m [4,5]. Parity-violating neutron spin rotation has been measured in certain heavy nuclei, where the

* Corresponding author. Present address: The George Washington University, Washington, DC 20052, USA.
E-mail address: amicherd@gwu.edu (A.M. Micherdzinska).

0168-9002/$ - see front matter © 2010 Elsevier B.V. All rights reserved.
doi:10.1016/j.nima.2010.11.105

effects are amplified [6–10], but uncertainties in nuclear structure make interpretation difficult.

A measurement of neutron spin rotation in ^{4}He was recently completed at the National Institute of Standards and Technology (NIST) Center for Neutron Research (NCNR) in Gaithersburg, Maryland. In any practical experiment, the spin rotation signal must be extracted from a much larger Larmor precession due to residual, longitudinal magnetic fields. To ensure that the neutron polarimetry can be performed to the required accuracy, we conducted an analysis of possible systematic effects and performed measurements to constrain the possible size of these effects and to characterize elements of the neutron polarimeter.

This paper reports measurements of phase space properties of the polarized cold neutron beam relevant to the measurement and their implications for systematic effects in the n-^{4}He spin rotation experiment. In Section 2, the neutron beam-line layout for the PV neutron spin rotation measurement is described. In Section 3, a subset of possible systematic effects involving polarimetry along with estimates of their sizes is discussed. This analysis indicates which beam properties need to be measured to place bounds on specific systematic effects. Section 4 presents results of the measurements and is divided into two subsections—the one for unpolarized beam properties (neutron capture flux and the beam intensity as a function of wavelength and spatial distribution) and the second for polarized beam properties (spatial images of polarization product, polarization product as a function of wavelength, rotation angle of supermirror analyzer, and area of the supermirror analyzer). The final section summarizes the results and implications for PV spin rotation measurements.

2. Neutron spin rotation beam-line and apparatus

2.1. Neutron source and spin rotation beam-line

At the NCNR, neutrons from a 20 MW reactor are moderated by a cold source and transported 68 m north along an evacuated rectangular ^{58}Ni-coated guide to the NG-6 end station [11]. The beam-line is oriented along a north–south axis with the neutrons traveling north. Local compass directions (north, south, east, west) will be used in the following sections to describe the position of a given object relative to the neutron beam.

After collimation and filtering, the neutrons pass through a 30 cm air gap and then enter the polarizing supermirror (PSM) [12], which polarizes the beam by transmitting only the neutrons that have magnetic moments parallel to the magnetic field of the device. Reflection from the PSM blades deflects the neutron beam approximately 15 mrad from the incident beam axis. The neutrons then enter an input neutron guide made of borosilica float glass consisting of two separate 1 m long sections. These guides have a critical reflection angle of 12 mrad/nm, which is small with respect to the critical angle of the NG-6 guide, so transmission of higher divergence neutrons is suppressed. Fig. 1 presents a diagram of the neutron beam-line and path along the spin rotation apparatus. It shows the magnetic field configurations used to maintain the neutron polarization upstream of the target and to manipulate the neutron polarization direction downstream of the target. Transverse neutron polarization after the PSM is maintained by a vertical field from magnetized soft iron plates located above and below the beam guide. The downstream end of the beam guide terminates inside the input coil, which nonadiabatically transports polarized neutrons into the magnetically shielded target region. The upstream end of the input coil is located outside of the magnetic shields for the target region, and the downstream end is placed within the magnetic shielding. Input and output coils have the shape of a rectangular prism. Both have a rectangular face oriented parallel to the beam direction with the longer edge along the beam direction.

The target region is followed by a few-centimeter air gap and then the output coil. The neutron polarization direction is manipulated in the output coil to achieve the crossed polarizer–analyzer configuration required for the measurement. Another float glass neutron guide with internal helium gas flow is located inside the output coil. Because the beam is divided into two sides (west and east), the output guide has a glass septum in the middle to prevent cross talk of neutrons between the two sub-beams. The small critical angle of the glass output guide rejects both higher divergence neutrons from the beam and neutrons scattered through large angles from the target walls.

After traveling through the output guide the beam reaches the polarization analyzing supermirror (ASM), whose blades have the

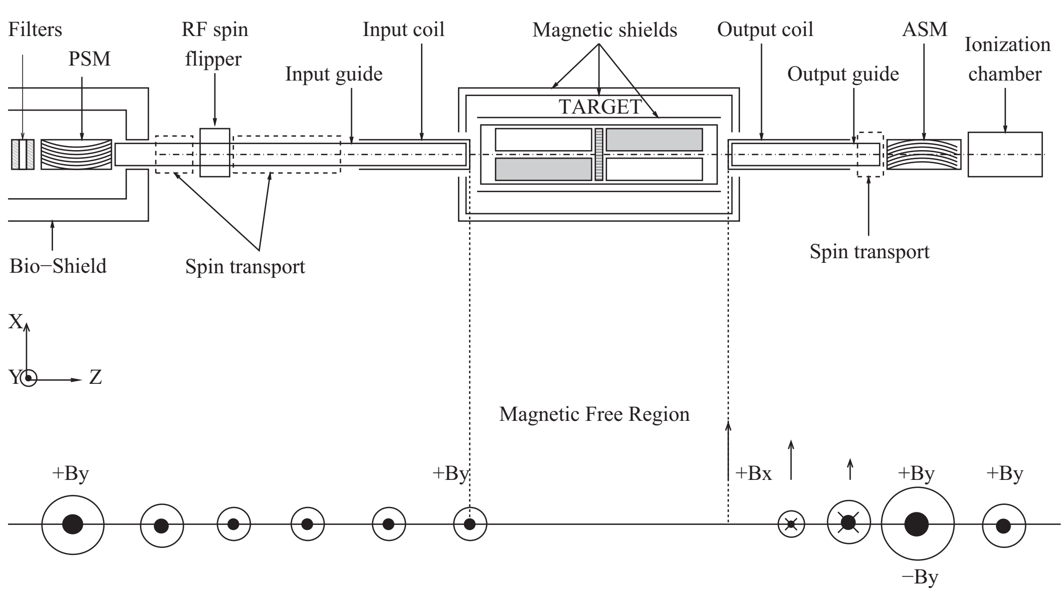

Fig. 1. Top view diagram of the spin rotation apparatus, and the magnetic fields throughout the apparatus. The target consists of four chambers and a π-coil. The bottom sketch indicates the magnitude and the direction of the magnetic field in each region of the apparatus. The dots show magnetic fields directed out of the page ($\hat{y}$), the cross means they point into the page ($-\hat{y}$).

same critical angle as the PSM. After leaving the ASM, neutrons enter an ionization chamber that operates in current mode and consists of four charge-sensitive plates along the beam direction [13,14]. Each of these plates is subdivided into four quadrants, so signals can be resolved spatially with respect to the top and bottom halves and the east and west halves of the beam. A detailed description of each part of the apparatus [14,15], and an outline of the measurement technique [16] may be found elsewhere.

3. Systematic effects dependent upon polarimeter and neutron beam phase space properties

To guide our consideration of which phase space properties of the beam need to be measured for a PV spin rotation measurement of 10^{-7} rad/m accuracy, one can organize anticipated sources of uncertainty into three classes: (a) multiplicative effects, which affect the scale of a true nonzero PV signal, (b) effects which increase the noise in the measurement significantly beyond the statistical limit given by $\sqrt{N}$, and (c) systematic effects which produce a nonzero signal in the experiment which are not due to PV spin rotation. In this section we discuss which properties of the neutron beam need to be analyzed with what accuracy to address effects (a) and (c). A full discussion of all possible systematic effects in spin rotation measurements is beyond the scope of this paper. Only the subset of the potential sources of systematic uncertainties associated with the dependence of the analyzing product signal on the polarized neutron beam phase space will be discussed.

By far the most serious systematic effects in PV spin rotation experiments with cold neutrons are associated, directly or indirectly, with longitudinal magnetic fields. A 10 nT longitudinal field gives a spin rotation of about 2 mrad in 1 m for a neutron of wavelength 0.5 nm. In our estimates of systematic effects associated with neutron polarimetry, we assume a 10 nT internal longitudinal magnetic field is present in the 1 m long target region. In this case if there is a systematic fractional difference in the magnetic field-induced rotations between the two target positions of 10^{-4}, then this effect is of the same size as the expected signal. Assuming the goal is to suppress all systematic effects to a size that is 1/10 of the expected size of the PV signal, the magnetic spin rotation for each target configuration is required to be the same to the 10^{-5} level.

3.1. *Systematic effects depending on non-ideal properties of the polarimeter*

Systematic uncertainties resulting from non-ideal properties of the polarimeter can depend on nonuniformities in the phase space properties of the neutron beam that couple to other asymmetries in the apparatus in a way that is difficult to characterize analytically. There is a clear need for subsidiary measurements to address these effects. In this section we estimate the order of magnitude of accuracy with which various phase space properties of the beam and the polarimeter must be measured and identify important issues to be addressed by the beam phase space measurements. We use specific properties of the liquid helium target in our estimates.

We can set the scale for the typical uniformity requirements for certain phase space properties of the beam as follows. In order to cancel the effects of a 10 nT residual field, which rotates the typical cold neutron by an angle of a few mrad, we need to limit the product of all nonuniformities which change the transmission intensity through the polarization analyzer at the 10^{-5} level. Due to the split beam, one needs a product of more than one of these nonuniformities to generate a systematic effect. Generally this means that we are interested in constraining the fractional nonuniformities of certain beam, target, or polarimeter properties at the 10^{-2}–10^{-3} level. Care must be taken in measuring those properties of the beam that are influenced by the target and are close to the edge of the acceptance of the polarimeter in any phase space variable, because this is a regime where the fractional changes can be large.

3.1.1. *Target-dependent neutron optical effects*

Consider the bending of neutron trajectories from gradients in the neutron optical potential due to gradients in target density. Such gradients can come from several possible sources such as gravity, pressure and temperature fluctuations, and static density nonuniformities in a solid. The time that the polarized neutrons in such bent trajectories spend in the residual field will be different for the two target positions and a different fraction of these trajectories will be accepted by the analyzer; in principle, this combination can generate a systematic effect.

As an example we estimate the angular deflection, θ, of the cold neutron beam in liquid helium (of length l) due to the gravity-induced density change, which is of order

$$\theta = \frac{l}{2}\frac{dV_{opt}}{dx}\frac{1}{E_k} \tag{2}$$

where E_k is the neutron kinetic energy and dV_{opt}/dx is the gradient in the neutron optical potential transverse to the direction of neutron motion. For liquid helium the liquid pressure changes by 10^{-3} (relative change) over the 5 cm height of the liquid in the beam. The liquid density, and therefore the neutron optical potential, changes by a similar amount (for liquid helium the compressibility at 4.2 K is close to 1). Such a fractional change in the 10 neV neutron optical potential of liquid helium acting over the 0.5 m target length bends the neutron beam up by an average angle of 30 nrad. For the apparatus geometry shown in Fig. 1, the difference in the fraction of neutrons accepted by the polarimeter from the upstream and downstream targets in the presence of the longitudinal field leads to an about 10^{-10} rad difference in the spin rotation angles accepted by the polarimeter in the two target states. It is clear from this estimate that one would need to amplify similar coherent neutron optical effects on the beam by 2–3 more orders of magnitude for this systematic to be of concern. The target nonuniformities needed to increase systematic effects of this type are difficult to maintain in a quasi-static liquid. The operating temperature throughout the experiment was 4 K [17].

Other systematic effects can come from target-dependent neutron refraction at the liquid-target chamber interface. Because the neutron momentum normal to the interface changes in the medium and the momentum component parallel to the interface does not, a neutron which crosses the boundary is spatially displaced along the boundary by an amount that is different for different neutron energies. As the liquid is moved in and out of the target chamber, the difference in the neutron index of refraction changes and therefore this spatial shift changes. Target-dependent shifts in the phase space of the beam from refraction effects are minimized in the target design by making the boundaries of all surfaces normal to the mean beam momentum [17]. Typical transverse neutron beam motion and angle shifts from the motion of the liquid and the target alignment tolerances are of order 10 nm and 1 μrad, respectively, and it is the difference in these numbers for the two targets (T_0 and T_1 target states) coupled with the residual field which is needed to generate a systematic effect. For this reason we are concerned with the spatial dependence of the analyzing power of the neutron polarization analyzer across the beam cross-sectional area. These measurements and the implications for the size of this systematic effect are presented and discussed in Section 4.2.1.

An important neutron optical systematic effect that is sensitive to the edges of phase space acceptance of the polarization analyzer comes from neutron reflection from the walls of the target. Because the critical angle for reflection is slightly different for an aluminum–liquid helium interface and an aluminum–helium gas interface and because in both cases these angles in principle lie within the phase space acceptance of the polarimeter (the critical angle for neutrons on glass is 12 mrad/nm, for neutrons on aluminum is 8 mrad/nm, and for the polarization analyzer is 40 mrad/nm), any change in the residual magnetic field seen by the neutrons close to the edges of the beam coupled with a target-dependent change in the beam phase space transmitted to the analyzer can lead to a systematic effect. Because the neutron optical potential of aluminum is 54 neV and the neutron optical potential of liquid helium is 10 neV, the difference in the critical angle for reflection from the two interfaces for a 0.5 nm neutron is 0.4 mrad, and the fraction of the beam that can be affected by this reflection is 10^{-3}. This possible systematic effect can be reduced significantly by introducing baffles into the target chamber to exclude wall-reflected neutrons from the phase space acceptance of the analyzer [17]. For neutrons that are blocked by the baffle structure, this suppresses the effect by at least the ratio of the total thickness of the baffles to the length of the target chamber, which is about $0.6\ \mathrm{cm}/50\ \mathrm{cm} \approx 10^{-2}$, and in reality this suppression will be much greater due to the large neutron absorption of the baffle material and the roughness of the surface it presents to the neutrons. Assuming a 10 nT field as above gives a 2×10^{-8} rad systematic effect under the stated assumptions.

3.1.2. Nonuniformities in the polarization product PA coupled to other phase space nonuniformities

Other systematic effects can come from nonuniformities in the polarization product PA of the beam polarization P and the analyzing power A of the ASM. The region of most rapid variation of this polarization product happens at the edges of the phase space acceptance of the supermirrors. Therefore, we designed the neutron optics so that none of the transmitted neutrons were close to this phase space edge. This was done using collimation to force the maximum divergence angle of the transmitted neutrons to lie within the phase space acceptance of the ASM and by the selection of the material for the neutron output guide, which was chosen to possess a smaller critical angle of reflection than the blades of the supermirror analyzer. These two choices ensure that unscattered neutrons are not close to the edge of the phase space acceptance of the ASM. This condition can be confirmed by measurements as discussed in Section 4.2.3.

There are also nonuniformities in the analyzing power of the ASM within its phase space acceptance due to its reflection-based design and its use of several stacked neutron mirrors to cover the full size of the beam. Nonuniformity of the supermirror analyzing power coupled with a target-dependent change in the neutron beam phase space accepted by the ASM can lead to a systematic effect. The neutron optical effects that can change the phase space of the unscattered beam are described in the Section 3.1.1. The estimated difference in the fraction of scattered neutrons that enter the ASM from the east and west target positions in our apparatus is approximately 10^{-6} based on the known neutron scattering cross-section of liquid helium. The phase space dependence of the analyzing power of the ASM within its acceptance therefore needs to be measured. These measurements and the size of the associated systematic effects are discussed in Section 4.2.2.

At a larger scale we also must be concerned with differences in PA between the two sub-beams. To achieve an accuracy close to neutron counting statistics in the face of extra beam intensity noise from the neutron source, the apparatus is split into two parallel experiments. The extraction of the PV signal requires an analysis that removes the common-mode noise present in both sub-beams. We therefore must be concerned with differences in the neutron beam phase space and PA between the two sub-beams. As an example of a systematic effect that can come from such differences, consider the quantity

$$[(PA_E - PA_W)_{T_0} - (PA_E - PA_W)_{T_1}] \cdot F \tag{3}$$

where PA_E and PA_W are the polarization products for the east and west sub-beams, T_0 and T_1 are the two different target states (with T_0 corresponding to liquid in the downstream target on the east side and the upstream target in the west side and T_1 is the reverse), and F is the fraction of scattered neutrons that enter the polarimeter. The term in parentheses is the target dependent part of the east/west asymmetry of the polarization products. If there is neither small angle scattering nor a spectrum shift, so that $F=0$, the only effect of east/west/T_0/T_1 dependencies of PA is to give slightly different multipliers to the observed count-rate asymmetries but not to generate a rotation angle where there was none to begin with. If F is nonzero and the scattered or energy-shifted neutrons are analyzed in the same way as the transmitted neutrons, then there is no effect. If there were a east-west symmetric target dependence to PA that could couple with scattered neutrons to generate a systematic effect, it would be a common-mode systematic. This effect will cancel in the calculation that removes common-mode noise and isolates the PV spin rotation angle. Thus this systematic effect is proportional to a product of three asymmetries.

In summary, these considerations of possible systematic effects indicate that we need to perform the following series of measurements to complete the estimates:

(1) PA as a function of neutron energy, beam location at the analyzer, and angular orientation of the analyzer for both sub-beams. The angular orientation measurements are needed to confirm the expected phase space acceptance of the ASM.

(2) PA as a function of the spatial location on the ASM. We need to make sure that the spatial variation of PA due to the reflection from the stacked blades in the ASM is not too large.

(3) Intensity and wavelength distribution across the beam. We needed to know the size of possible nonuniformities in these beam properties to estimate possible systematic effects coming from any nonuniformities seen in (1) and (2).

4. Beam measurements

4.1. Unpolarized beam measurements

4.1.1. Wavelength distribution

We measured the neutron wavelength distribution by chopping the beam and measuring the time dependence of the neutron intensity at a known distance. The chopper is made of ^{6}LiF plastic glued to a phenolic disk and has two apertures located at a radius of 15 cm. The beam defining apertures are 3.8 mm wide, and the disk rotates at 60 Hz. The neutrons were detected by a 10 cm $\times$ 10 cm, 0.4 mm thick ^{6}Li/ZnS(Ag) scintillator coupled to a photomultiplier tube. Backgrounds were measured by absorbing the neutron beam in ^{10}B-loaded polymer sheet. The time-of-flight spectrum is converted to a beam wavelength distribution by using both the beam-line geometry and our prior knowledge of the origin of various features of the spectrum. Certain notches and discontinuities in the NG-6 neutron spectrum are caused by diffraction from upstream material in the beam, including magnesium in the beam windows, a graphite monochromator with wavelength selections at 0.48 and 0.6 nm, a beryllium filter with cutoff wavelength of 0.398 nm, and a bismuth filter. Fig. 2 shows our measured neutron wavelength distributions measured before and after the PSM.

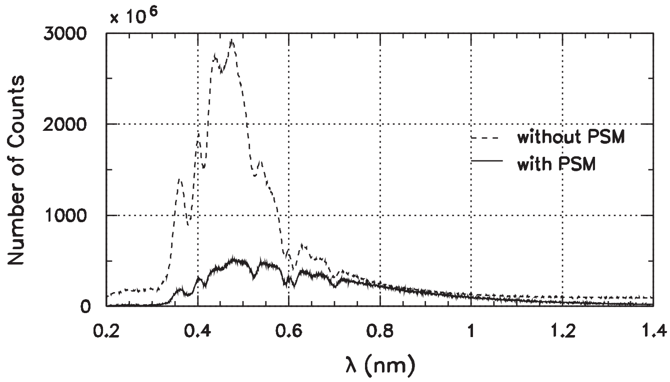

Fig. 2. Neutron wavelength distribution measured at NG-6, before and after the PSM. Calibration of the time-of-flight scale for the measurement was done using geometry and also using notches in the distribution from diffraction by upstream crystals and matter of known composition and structure in the beam.

Other measurements of the wavelength distribution of the polarized beam were performed to characterize the neutron polarization devices. These measurements were performed in the same way and are presented in Section 4.2.3.

4.1.2. Spatial distribution of neutron intensity

The relative neutron intensity distribution across the beam was measured using a neutron imager [18]. Two methods of developing the neutron image were employed. One uses a commercially available neutron image plate consisting of a powder mixture of BaFBr:Eu^{2+} and Gd_2O_3 dispersed in a polymer matrix and supported by a flexible polymer sheet. Although this image plate material makes possible a one-step process to extract the image, because BaFBr:Eu^{2+} is an excellent X-ray storage phosphor, it is also sensitive to γ-radiation, which is always present as a background radiation in neutron experiments. The other technique uses a material with a high neutron capture cross-section, a decay branch into betas, and a convenient half-life. We used a 10 cm $\times$ 10 cm foil of natural dysprosium. After irradiation, the decay electrons from neutron absorption in ^{164}Dy expose a film that is sensitive to electrons and can be read out by an image reader. The pixel resolution of the image reader is 200 μm $\times$ 200 μm. Images were taken immediately after the PSM, after the input guide and input coil, and after the output guide and output coil. Images are presented in Fig. 3. The intensity scale of the images is linearly proportional to the neutron fluence; however, the proportionality factor is different for each image because the irradiation time was not the same.

The beam after the PSM is not uniform. Not only does one see the PSM blades and the wires of the input coil, but there is also a horizontal intensity gradient across the face of the PSM of about 15% The image after the output guide and coil shows that the right side is about 20% more intense, consistent with the initial non-uniformity in the beam seen just after the PSM. Because the measured spin rotation is calculated from asymmetries, the intensity difference alone does not produce systematic effects. However, a spatial gradient in the intensity across the beam might couple to other beam phase space nonuniformities which could pose a problem.

4.1.3. Neutron fluence measurement

We used a calibrated ^{235}U fission chamber to measure neutron fluence at various positions along the apparatus. The fission chamber operated in pulse-counting mode with an efficiency of 10^{-7}. The absolute accuracy of this device is approximately 5%. A detailed description of the fission chamber can be found in Ref. [19].

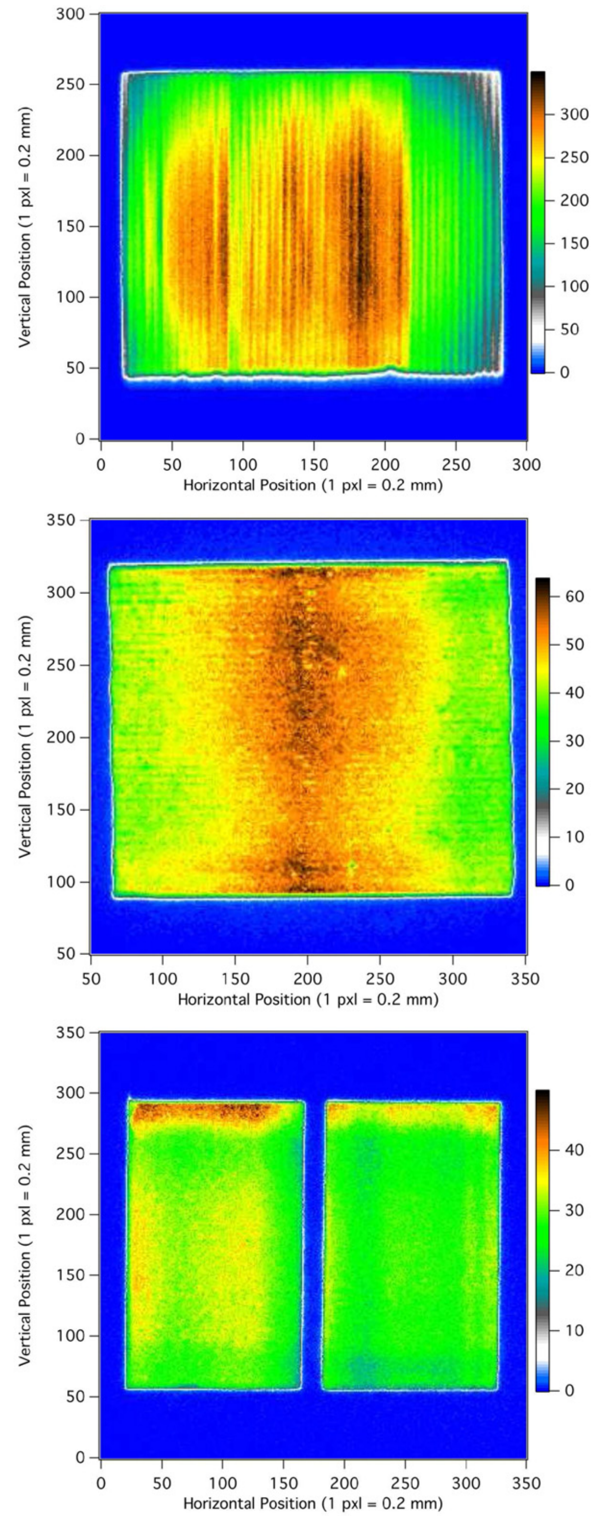

Fig. 3. Beam images. The top image was taken just downstream of the polarizing supermirror. The vertical pattern is due to the blades of the supermirror. The middle image was obtained downstream of the input coil, just before entering the target region. The horizontal pattern results from the wires of the input coil. The bottom image was taken between the output guide and the analyzing supermirror. The beam was divided into two halves in the target region by the collimation.

The sensitive area of the fission monitor is a disc with a diameter of 12 mm. Because this does not cover the full beam, we used two different methods to extrapolate the measurements to the equivalent full beam values: (a) measurements were performed in different locations across the beam and averaged, (b) one

Table 1
Average value of neutron capture flux measured and simulated at different positions along the spin rotation apparatus. Capture flux is the integral of the flux over the velocity distribution in the beam weighted by a factor v_0/v which takes into account a typical velocity dependence for neutron absorption in the detector, $v_0 = 2200$ m/s by convention.

Measurement position	Neutron flux ($cm^{-2} s^{-1}$) (measurement)	Neutron flux ($cm^{-2} s^{-1}$) (simulation)
Before PSM	1.2×10^9	No data
After PSM	3.1×10^8	3.1×10^8
After input coil	1.5×10^8	1.6×10^8
Before ASM	0.5×10^8	0.5×10^8

measurement was performed in a known location in the beam and combined with a full beam image to determine the relative intensities. The average neutron flux at various positions along the spin rotation apparatus determined in this manner is presented in Table 1. We also performed Monte Carlo simulations [20], where the properties of the target, polarized beam, and the experimental geometry were implemented. The simulations assumed the idealized model of the phase space properties of the beam and included the geometry and neutron optical properties of the polarizer, analyzer, input and output guides, and beam geometry and collimation. The simulation is therefore only expected to be capable of describing some gross features of the beam evolution along the apparatus such as the intensity.

For relative fluence measurements, described in Section 4.2, non-calibrated fission chambers of 50 mm $\times$ 50 mm area that were able to cover the full beam were used.

4.2. Polarized beam measurements

The most important parameter of the polarizer–analyzer pair for neutron polarimetry is its polarization product *PA*, the product of the polarizing power *P* of the polarizer and the analyzing power *A* of the polarization analyzer. *PA* is measured by placing a non-adiabatic neutron spin flipper between the PSM and the ASM measuring the relative transmission rates

$$PA = \frac{N_u - N_f}{sN_u + N_f} \tag{4}$$

where N_u and N_f are the neutron intensities transmitted through the polarizer/analyzer pair with the spin in the unflipped or flipped state, respectively. The spin flip efficiency s is 0.95 ± 0.05, as determined in another experiment [21].

Measurements presented in this section are similar in character to those performed for other polarized cold neutron experiments [21,22].

4.2.1. Spatial image of PA

This measurement was performed by taking two beam images after the PSM and ASM with a nonadiabatic spin flipper between them turned either on or off. The nonadiabatic spin flipper consisted of two parallel coils, with the first coil generating a magnetic field pointing in $+\hat{y}$–direction and the second coil generating a magnetic field in $+\hat{y}$- or $-\hat{y}$–directions. The setup for this measurement is presented in Fig. 4. From these measurements and the known spin flip efficiency over the NG-6 beam-line wavelength (95%, [21]), we determined *PA* across the face of the ASM and the results are presented in Fig. 5.

The blades of the supermirror introduce nonuniformities in *PA* of approximately 5%/mm and 1%/mrad. These values represent a typical change in *PA* for a neutron originating in a target and subsequently entering the analyzer. The quantities are obtained using the distance of the target to the ASM and the data provided in the images of Fig. 5.

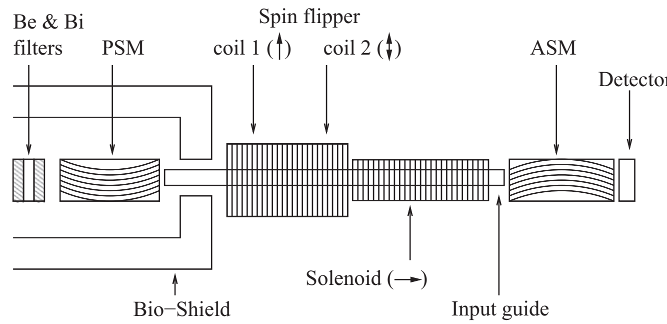

Fig. 4. Sketch of experimental apparatus used for *PA* beam image measurement using a nonadiabatic spin flipper. Arrows indicate the direction of the magnetic field. For coil 2, the direction of the magnetic field was flipped every second.

We use these values to complete our estimate of the size of the systematic effects from beam refraction. The systematic effect from the transverse beam motion (10 nm and 1 μrad, see discussion in Section 3.1.1) coupled with the nonuniformity in the analyzing power is therefore less than 10^{-8} rad for transverse beam motion and less than 10^{-8} rad for angular deviations, thereby constraining these effects to be an order of magnitude smaller than the sensitivity goal of the experiment.

4.2.2. Polarization product as a function of energy, angle, and location in the beam

Fig. 6 shows the experimental setup used for the measurements. Up to the magnetic shielding, it is the same setup as presented in Fig. 1. Additionally, the ASM was placed immediately after the input coil and a pulse-counting ^{3}He detector attached to the end-face of the ASM. The detector consists of a rectangular aluminum chamber of dimensions 51×51 mm^2 and a height of 76 mm, filled with ^{3}He gas under a pressure of 0.4 MPa. The rectangular shape of the ^{3}He detector ensures uniformity of the detector efficiency across the detector acceptance. The ^{3}He detector is shielded on all surfaces not viewing the direct beam with neutron-absorbing materials containing either ^{6}Li or ^{10}B. The unshielded 38 mm $\times$ 51 mm rectangular aperture on the face of the detector was connected to the downstream face of the ASM. A ^{10}B mask with a vertical 5 mm wide $\times$ 50 mm long slit was attached to the downstream end of the input coil to sample different sections of the beam. Measurements were performed for three positions of the collimation slit, in the middle, on the west, and on the east side of the original collimation of the input coil.

First we removed the chopper and measured the dependence of *PA* on the horizontal divergence angle (defined as the angle of the neutron trajectory relative to the beam centerline) by rotating the ASM about a vertical axis. This measurement was done with the ^{10}B collimation slit on the middle, on the east, and on the west side on the downstream end of the input coil. Fig. 7 presents the transmissions for both spin states together with *PA* for different analyzer angular orientations relative to the beam centerline. The orientation corresponding to 0 mrad is chosen to maximize the transmitted intensity when the collimator was placed in the middle of the input coil.

PA is approximately constant over the range ± 20 mrad with no sharp nonuniformities in its analyzing power. Given the wavelength distribution of the incident beam from the ^{58}Ni guide (Fig. 2), the dimensions and critical angles of the glass guides between the polarizer and analyzer (12 mrad/nm), and the collimation in the output guide, the maximum neutron wavelength which can enter the ASM either by

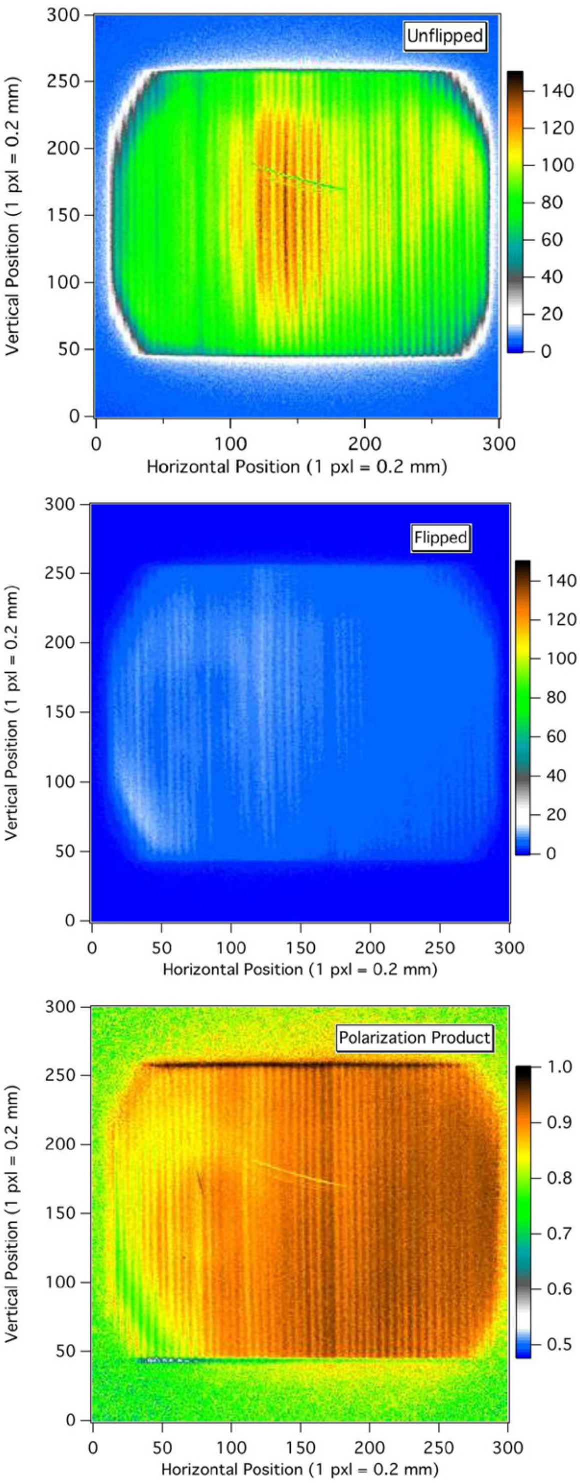

Fig. 5. Beam images. The top panel shows the beam image with the spin flipper in the unflipped state. The middle panel shows the beam image with the spin flipper in the flipped state. The intensity scale is arbitrary, but both images are normalized to the same exposure time. The bottom panel shows an image of the polarization product generated from the first two images using Eq. (4). The region outside the outline made by the supermirror has no significance.

transmission or by scattering is 1.0 nm. Coupled with the known reflectivity of the supermirrors that possess high reflectivity out to an angle twice that for natural nickel, one expects that the analyzing power of the polarization analyzer will decrease for angular orientations greater than 20 mrad, which is precisely what is observed. This

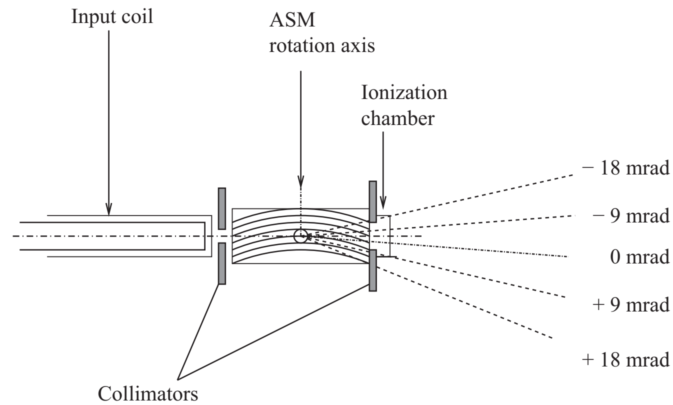

Fig. 6. Sketch of experimental apparatus used for measurements of the polarization products as a function of ASM rotation angle α, position in the beam, and wavelength. Collimators were shifted to define the region of the analyzer to be measured. The collimated proportional counter was placed in three positions (east, middle and west).

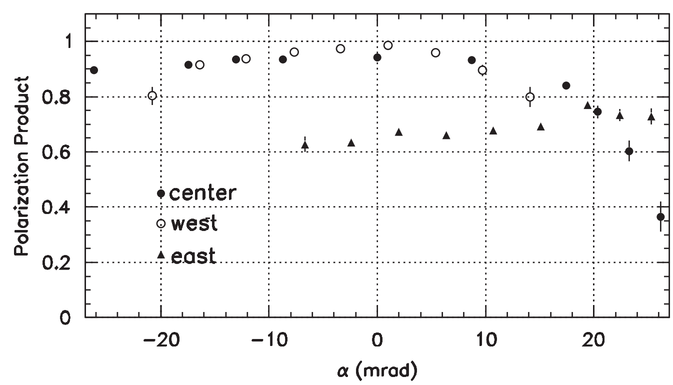

Fig. 7. Polarization product as a function of the rotation angle α of the ASM for west, central and east positions.

measurement therefore confirms that the phase space of the transmitted and scattered polarized neutron beam is well within the phase space acceptance of the ASM, and therefore eliminates the potential systematic effect described in Section 3.1.2.

Note the smaller value of the polarization product for the east portion of the beam compared to the central and west portions of the beam. For east and west sides of the beam, the polarization product is $\approx 60\%$ and 80% (within the 5% uncertainty), respectively. The observed east/west asymmetry in the polarization products is therefore of order 10%. The origin of this nonuniformity is not understood. Although this does not by itself generate a systematic effect, it can couple to other beam phase space nonuniformities and produce the systematic effect discussed in Section 3.1.2 that is associated with the target dependence of the east/west asymmetry of the polarization products. From our measurement we can estimate the size of this systematic effect. Because the estimated difference in the fraction of scattered neutrons which enter the analyzer from the two target positions is about 10^{-6}, the east/west asymmetry of the polarization products from this measurement is 0.1, and the precision with which the polarization products should be equal for the two target states T_0 and T_1 (which are necessarily measured at different times) is expected to be approximately 10^{-3} radians from magnetic field drifts, the upper bound on the size of this systematic effect is 10^{-10} radians, which is negligible.

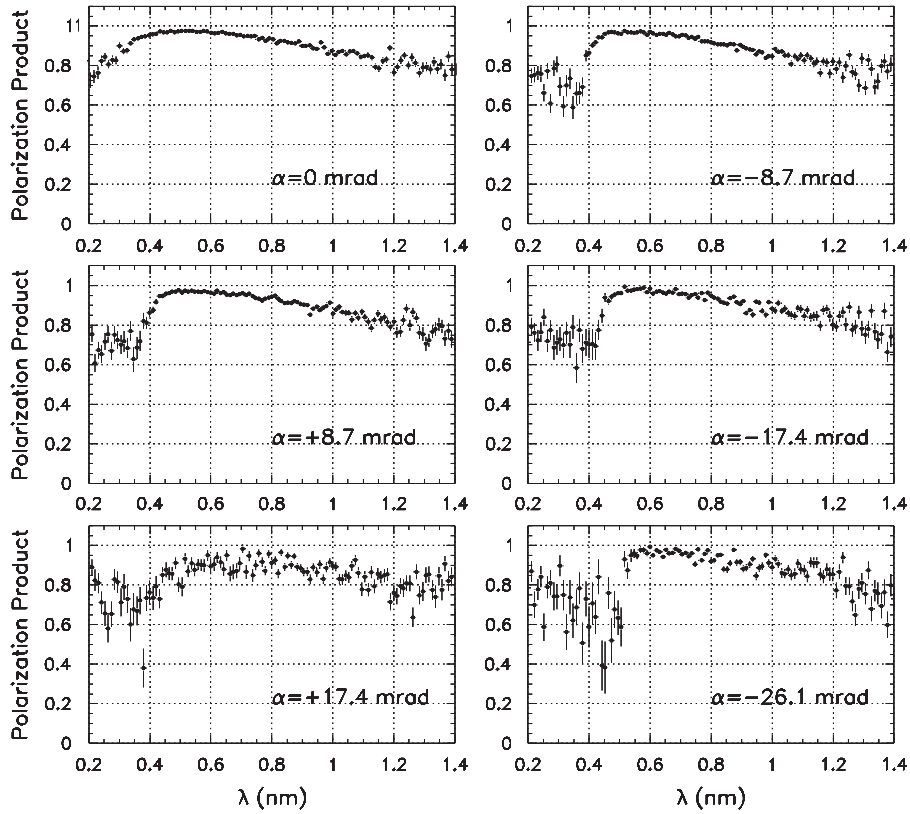

Fig. 8. Polarization product as a function of wavelength for the collimator slit in the central position. The ASM is rotated by an angle $\alpha=0$, +8.7, +17.4, −8.7, −17.4 and −26.1 mrad. Rotation angles are presented in Fig. 6. $\alpha=0$ mrad is a nominal position.

4.2.3. Polarization product as a function of wavelength and ASM cross-section area

Figs. 8 and 9 show the polarization product as a function of wavelength for measurements taken with collimator slit in the center, east, and west of the beam. The same experimental setup with a chopper as described in Section 4.1.1 was used for these measurements. In each case the zero for the ASM position is defined by the angular position at which the maximum fluence was found during the previous measurements.

The *PA* is fairly constant across the wavelength distribution and as a function of the ASM angle. This justifies the analysis of the systematic effects in which we assumed that the analyzing power of entering neutrons is independent of neutron energy and angle. Although there are some rapid changes in *PA* for neutrons of wavelengths below 0.4 nm, there is little statistical weight in the polarized neutron beam spectrum in this range. The small shift in the edge of the wavelength distribution near 0.4 nm, which is efficiently analyzed as the analyzer is rotated away from the optimum angle, is also as expected. The measured behavior of the east section of the beam is qualitatively different from the center and west sections of the beam as noticed earlier. As can be seen in the wavelength dependence of *PA*, the origin of this difference is due to a significant transmission of the wrong spin state on the east section of the beam. This problem is not present in the other measured beam locations.

We have shown that the *PA* is uniform within the wavelength distribution, but is not uniform across the spatial cross-section of the end-face of the ASM. This implies that the measurement has to be done on each side of the beam independently to properly calibrate the spin angle. The ionization chamber for the PV experiment is segmented into 4 quadrants × 4 sectors along its length. This segmentation allows us to measure *PA* independently for each of the four quadrants. This includes four integrated wavelength distributions, which the different longitudinal segments of the chamber are sensitive to. In the spin rotation experiment, *PA* is periodically measured by tilting the input guide by known angles to produce a large neutron spin angle that can be quickly analyzed by the polarization analyzer.

5. Summary

In this paper we described the design of a neutron polarimeter used to search for parity-violating spin rotation with sensitivities approaching 10^{-7} rad/m. We identified possible systematic effects whose sizes depend in detail on the interaction between polarized neutron beam properties and the apparatus. These are difficult to characterize theoretically, and therefore we limited this class of systematics by measurement.

We performed an extensive set of measurements on the NG-6 neutron beam-line to characterize these beam-related systematics. This set includes the following measurements: intensity distribution as a function of the neutron wavelength; absolute intensity distribution at several locations along the polarimeter; intensity distribution and energy spectrum of the polarized neutron beam; *PA* of the PSM and ASM as a function of neutron energy, location in the beam, and the angular orientation of the analyzer. On the basis of these measurements, we summarize the following features of the beam:

1. The wavelength distribution is close to the expected Maxwellian shape from 0.35 to 1.0 nm with a maximum at 0.45 nm.
2. The neutron intensity right after the PSM for the east and west side of the beam is not the same. The intensity difference is approximately 20%. This asymmetry does not by itself lead to a systematic effect. However, it could in principle couple to

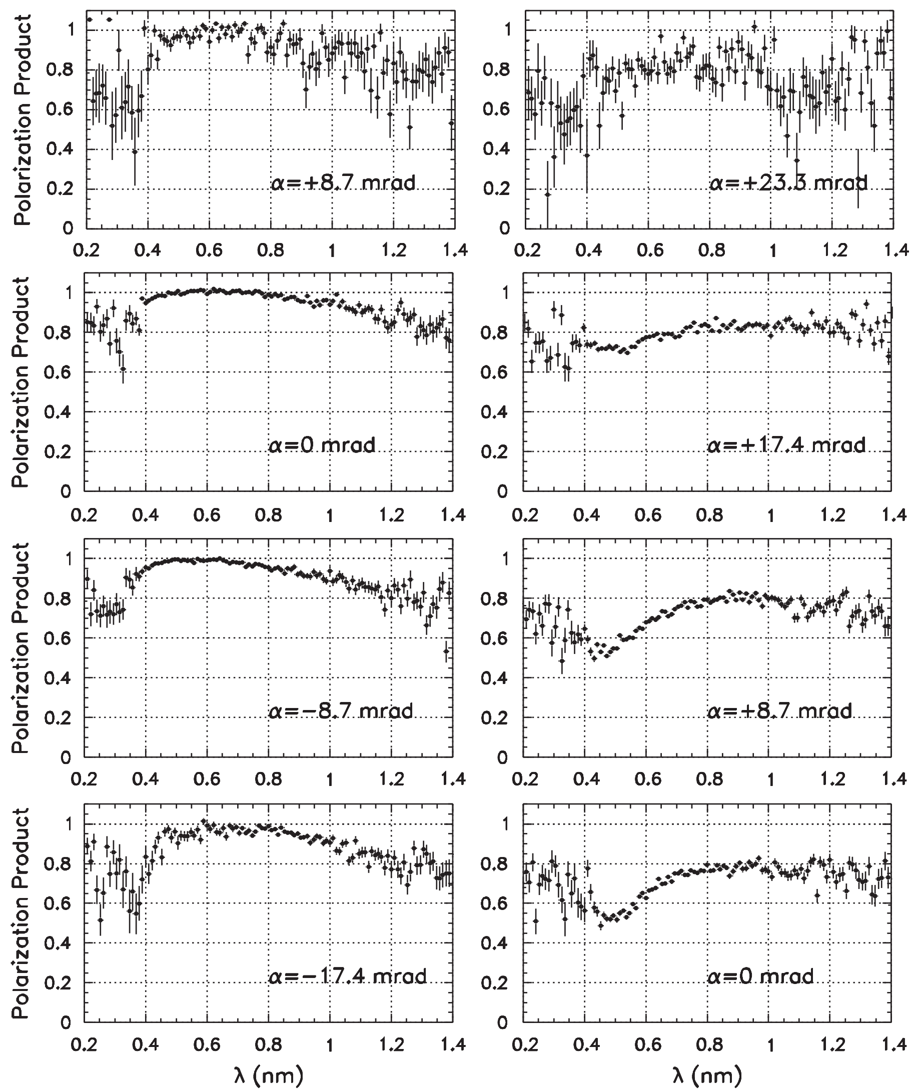

Fig. 9. Same as in Fig. 8 but for the collimator slit in the west position (left panel), and in the east position (right panel). For the collimator slit in the west position the rotation angles α are: +8.7, 0, −8.7 and −17.4 mrad; for the collimator slit in the east position the rotation angles α are +23.3, +17.4, +8.7 and 0 mrad.

another beam phase space asymmetry. Measurements of the linearity of the ^{3}He-ionization chamber response over the range of neutron beam intensities encountered in the measurement are needed to limit certain systematic effects.

3. *PA* for the east and west sides of the beam differs by 20%, but as noted, this difference by itself does not necessarily lead to a systematic effect. As long as one determines the spin rotation angle for each of the four beam quadrants and corrects the *PA* of the four longitudinal segments of the ionization chamber, the systematic contribution is negligible.
4. The measurements of the spatial uniformity of *PA* show that nonuniformities of about 5%/mm and 1%/mrad in the horizontal plane exist in the analyzing power of the supermirror due primarily to the edges of the blades.
5. *PA* for the different locations in the beam as a function of the orientation of the ASM shows that the edges of the phase space acceptance of the supermirrors are at ± 20 mrad, which is consistent with expectations taking into account the spectrum of the NG-6 beam and the reflectivity of the supermirrors. This angle is larger than the 12 mrad maximum reflection angle under which neutrons will enter the ASM, which is set by the beam collimation and neutron optical potential of the glass output guide. Therefore the phase space of the beam entering the polarization analyzer does not encounter any rapid variations beyond the ones already known to exist based on the mirror blades in the analyzer.
6. *PA* for the different measured locations in the beam varies slowly as a function of neutron energy for the energy range of the neutron spectrum used in the measurement.

Table 2
Estimated size of the systematic effects for the n-^{4}He neutron spin rotation experiment on the NG-6 beam-line: neutron refraction effects due to target nonuniformities (neutron refraction #1), target-dependent neutron refraction at the liquid-target chamber interface (neutron refraction #2), target position-dependent neutron reflection from internal surfaces (neutron reflection), and target dependence of polarization products (polarization product).

Systematic effect	Size (rad)
Neutron refraction #1	10^{-10}
Neutron refraction #2	10^{-8}
Neutron reflection	2×10^{-8}
Polarization products	10^{-10}

With these measurements and the analysis of the systematic effects presented in Section 3, we can estimate the sizes of the systematic effects for the spin rotation experiment. These effects are presented in Table 2. We did not find any systematic effects associated with the polarized beam characteristics that would pose a significant problem for spin rotation measurements at the 10^{-7} rad/m level of precision. Work is in progress on a more extensive characterization of target-related systematic effects and measurements that place limits on possible systematic effects associated with the ionization chamber. We note that the measurements and analysis techniques described here are applicable to neutron spin rotation experiments in other target materials, such as hydrogen or deuterium. Because the neutron beam phase space nonuniformities depend on the neutron scattering dynamics in the target and the polarimeter nonuniformities are device specific, an analysis similar in form but different in details to that presented in this paper would be required to judge the possibility of performing parity-odd neutron spin rotation measurements in H or D.

Acknowledgments

This work was supported in part by NSF PHY-0457219, NSF PHY-0758018, and a US Department of Energy Grant DE-FG02-95ER40901 and interagency agreement DE-AI02-93ER40784. The authors acknowledge the support of the National Institute of Standards and Technology, The U.S. Department of Commerce, in providing the neutron facilities used in this work. The authors acknowledge support from the Indiana University Center for Spacetime Symmetries. The authors also acknowledge the Kazakhstan Ph.D. program at the Al-Farabi Kazakh National University, which allowed Ph.D. student V. Zhumabekova to participate in these measurements.

References

[1] L. Stodolsky, Nucl. Phys. B 197 (1982) 213.
[2] W.M. Snow, J. Res. Natl. Inst. Stand. Technol. 110 (2005) 189.
[3] D.M. Markoff, J. Res. Natl. Inst. Stand. Technol. 110 (2005) 209.
[4] B. Desplanques, J. Donoghue, B. Holstein, Ann. Phys. 124 (1980) 449.
[5] B. Heckel, The investigation of fundamental interactions with cold neutrons, in: G.L. Greene (Ed.), NBS Special Publication, vol. 711, 1986, p. 90.
[6] M. Forte, et al., Phys. Rev. Lett. 45 (1980) 2088.
[7] B.R. Heckel, et al., Phys. Lett. B 119 (1982) 298.
[8] B.R. Heckel, et al., Phys. Rev. C 29 (1984) 2389.
[9] S. Saha, Parity nonconserving spin rotation in bromine, cesium and rubidium, Ph.D. Thesis, University of Washington, Seattle, 1990.
[10] T. Haseyama, et al., Phys. Lett. B 534 (2002) 39.
[11] J.S. Nico, et al., J. Res. Natl. Inst. Stand. Technol. 110 (2005) 137.
[12] O. Schaerpf, Phys. B Condens. Matter 156 (1989) 631; O. Schaerpf, Phys. B Condens. Matter 156 (1989) 639.
[13] S.D. Penn, et al., Nucl. Instr. and Meth. A 457 (2001) 332.
[14] D. Luo, Measurement of the parity non-conserving spin rotation of cold neutrons through a liquid helium target, Ph.D. Thesis, Indiana University, Bloomington, 2009.
[15] D.M. Markoff, Measurement of the parity nonconserving spin-rotation of transmitted cold neutrons through a liquid helium target, Ph.D. Thesis, University of Washington, Seattle, 1997.
[16] W.M. Snow, Nucl. Instr. and Meth. A 611 (2009) 248.
[17] C.D. Bass, et al., Nucl. Instr. and Meth. A 612 (2009) 69.
[18] M. Schlapp, et al., J. Phys. D Appl. Phys. 37 (2004) 2607.
[19] J.A. Grundl, et al., Nucl. Technol. 25 (1975) 237.
[20] M. Sarsour, Internal Report, IUCF, 2004—Simulation for Neutron Spin Rotation, 2003.
[21] H.P. Mumm, et al., Rev. Sci. Instrum. 75 (2004) 5343.
[22] J. Zejma, et al., Nucl. Instr. and Meth. A 539 (2005) 622.